

Can one-zone hadronuclear model explain the hard-TeV spectrum of BL Lac objects?

Wei-Jian Li¹, Rui Xue¹, Guang-Bo Long², Ze-Rui Wang³, Shigehiro Nagataki^{4,5}, Da-Hai Yan^{6,7}, and Jian-Cheng Wang^{6,7}

¹ Department of Physics, Zhejiang Normal University, Jinhua 321004, People's Republic of China
e-mail: rui.xue@zjnu.edu.cn

² School of Physics, Sun Yat-sen University, Guangzhou, Guangdong, People's Republic of China

³ College of Physics and Electronic Engineering, Qilu Normal University, Jinan 250200, People's Republic of China

⁴ Astrophysical Big Bang Laboratory (ABBL), RIKEN, Saitama 351-0198, Japan

⁵ Interdisciplinary Theoretical & Mathematical Science Program (iTHEMS), RIKEN, Saitama 351-0198, Japan

⁶ Yunnan Observatories, Chinese Academy of Sciences, Kunming 650011, China

⁷ Key Laboratory for the Structure and Evolution of Celestial Objects, Chinese Academy of Sciences, Kunming 650011, China

Received xxx; accepted xxx

ABSTRACT

Context. The intrinsic TeV emission of some BL Lacs are characterized by a hard spectrum (the hard-TeV spectrum) after correcting for the extragalactic background light. The hard-TeV spectra pose a challenge to conventional one-zone models, including the leptonic model, the photohadronic model, the proton synchrotron model, etc.

Aims. In this work, we study if the one-zone hadronuclear (pp) model can be used to interpret the hard-TeV spectra of BL Lacs without introducing extreme parameters.

Methods. We give analytical calculations to study if there is a parameter space and the charge neutrality condition of jet can be satisfied when interpreting the hard-TeV spectra of BL Lacs without introducing a super-Eddington jet power.

Results. We find that in a sample of hard-TeV BL Lacs collected by Xue et al. (2019a), only the hard-TeV spectrum of IES 0229+200 could be explained by γ -ray from π_0 decay produced in the pp interactions, but at the cost of setting a small radius of the radiation region that comparable to the Schwarzschild radius of the central black hole. Combining with previous studies of other one-zone models, we suggest that the hard-TeV spectra of BL Lacs cannot be explained by any one-zone models without introducing extreme parameters, and should originate from the multiple radiation regions.

Key words. galaxies: active – galaxies: jets – radiation mechanisms: non-thermal

1. Introduction

Blazars are a class of active galactic nuclei (AGNs) with their relativistic jets pointing to the observer (Urry & Padovani 1995). Combining with multi-wavelength observations, it is found that the spectral energy distributions (SEDs) of blazars usually exhibit two characteristic bumps. It is generally accepted that the low-energy bump originates from the synchrotron radiation of primary relativistic electrons in the jet. While, the origin of the high-energy bump is under debate. In leptonic models, the high-energy bump is explained by inverse Compton (IC) radiation from relativistic electrons that up-scatter soft photons emitted by the same population of electrons (synchrotron-self Compton, SSC; Marscher & Gear 1985), or soft photons from external photon fields (external Compton, EC) such as the accretion disk (Dermer & Schlickeiser 1993), the broad-line region (BLR, Sikora et al. 1994) or the dusty torus (DT, Błażejowski et al. 2000). In hadronic models, the high-energy bump is supposed to be originated from proton synchrotron radiation (Ahoronian 2000), emission from secondary particles generated in photohadronic processes ($p\gamma$) including photopion and Bethe-Heitler pair production processes (Sahu et al. 2019), and the internal $\gamma\gamma$ pair production, or cascade emission generated in the intergalactic space through $p\gamma$ interactions by ultra-high energy cosmic

rays (UHECR) with energies up to 10^{19-20} eV beamed by the blazar jet (e.g., Essey et al. 2011).

The extragalactic TeV background is dominated by emission from blazars (Ackermann et al. 2016), most of which are BL Lacertae objects¹ (BL Lacs; Urry & Padovani 1995). After correcting for the extragalactic background light (EBL) absorption, the obtained intrinsic TeV emission of some BL Lacs often shows a hard spectrum, i.e., the photon index $\Gamma_{\text{TeV}} < 2$ (hereafter the hard-TeV spectrum). However, some intrinsic TeV spectra are too hard to be interpreted by conventional radiation models. In the modeling of blazars' radiation, it is usually assumed that all the jet's non-thermal emission comes from a compact spherical region, named blob. Such a model is also known as the one-zone model, where the one-zone leptonic model is the most commonly used (e.g., Ghisellini et al. 2014; Tan et al. 2020; Deng et al. 2021). However, since the Klein-Nishina (KN) effect softens the IC emission in the TeV band naturally, the one-zone leptonic model cannot reproduce the hard-TeV spectrum unless setting an extremely high Doppler factor (e.g., Aleksić et al. 2012), which is in conflict with radio observations (Hovatta et al. 2009), and/or introducing a very high value of the minimum electron Lorentz factor (e.g., Katarzyński et al.

¹ <http://tevcat.uchicago.edu/>

2006). In the modeling of blazars, the one-zone $p\gamma$ model is also widely applied. To explain the hard-TeV spectrum, an extremely high proton power is required since the $p\gamma$ interaction is very inefficient. Based on the fact that the interaction efficiency of the photopion process in the high-energy limit is about 1000 times smaller than the bump of $\gamma\gamma$ opacity, Xue et al. (2019a) prove that the required minimum jet powers of a sample of hard-TeV BL Lacs exceed the corresponding Eddington luminosities of the supermassive black holes (SMBHs). For the emitting region with a strong magnetic field (10–100 G), the one-zone proton synchrotron model is also widely applied to explain the high-energy bump (Böttcher et al. 2013). However, the super-Eddington jet power is also needed (Zdziarski & Böttcher 2015) except for some few cases such as the fast variabilities ($t_v \leq 10^3$ s; Petropoulou & Dermer 2016) and very hard injection functions ($\alpha \leq 1.5$; Cerruti et al. 2015). In addition, some studies suggest that the magnetic field in the inner jet of blazars is typically lower than 10 G (O’Sullivan & Gabuzda 2009; Meyer et al. 2014). If the hard-TeV spectrum is still explained by the proton synchrotron emission in a magnetic field $\lesssim 10$ G, the maximum proton energy larger than that obtained from the Hillas condition (E_{Hillas} ; Hillas 1984) has to be assumed. The cascade emission from the UHECR can explain the hard-TeV spectrum either, but may also needs extremely high maximum proton energy higher than E_{Hillas} (Takami et al. 2016, cf., Das et al. (2020)). Also, the hard-TeV spectra of some BL Lacs show variabilities (e.g., Acciari et al. 2010), which disfavour the cascade emission from UHECR (e.g., Prosekin et al. 2012). Over all, the hard-TeV spectra pose a challenge to conventional one-zone models.

In various one-zone models introduced above, the one-zone hadronuclear (pp) model has not been studied comprehensively. In the study of radiation mechanisms of blazars’ jet, the pp interaction is normally neglected, since the particle density in the jet is considered not sufficient (Atoyan & Dermer 2003). Recently, several associations between high-energy neutrinos and blazars are discovered (e.g., IceCube Collaboration et al. 2018). However, these events are difficult to be explained by the conventional one-zone $p\gamma$ model (e.g., Xue et al. 2019b, 2021), therefore several innovative pp models are proposed (e.g., Sahakyan 2018; Banik & Bhadra 2019; Liu et al. 2019; Wang & Xue 2022a). Also, Xue et al. (2019a) suggest that the one-zone pp model may provide a possible solution to reproduce the hard TeV spectrum with a sub-Eddington jet power, since the efficiency of pp interactions is not related to the opacity of $\gamma\gamma$ absorption. Therefore, further considering the pp interaction in the one-zone model comprehensively is a necessary complement to understand the origin of hard-TeV spectra of BL Lacs.

In this paper, we will analytically study whether the hard-TeV spectra of BL Lacs can be explained without violating basic observations and theories in one-zone pp models. In Section 2, we present analytical methods to find the parameter space, and then study if the charge neutrality condition can be satisfied in the framework of one-zone pp models. We present the discussion and the conclusion in Section 3. Throughout the paper, the Λ CDM cosmological parameters $H_0 = 70 \text{ km s}^{-1} \text{ Mpc}^{-1}$, $\Omega_m = 0.3$, $\Omega_\Lambda = 0.7$ are adopted.

2. Analytical calculations

For blazar jets, the pp process is usually considered in interactions between the jet and its surrounding materials, such as dense clouds in the BLR, and red giant stars captured from the host galaxy (e.g., Bosch-Ramon et al. 2012). However, it is unclear if the jet inside has sufficient cold protons. Here, we propose

analytical methods to study if the hard-TeV spectra of BL Lacs can be explained by the one-zone pp model, which considering the pp interactions occur in the jet without introducing extreme parameters. We also study if the charge neutrality condition of jet can be satisfied, although this commonly assumed condition (Ghisellini et al. 2014) is under debate at present (Chen & Zhang 2021).

It should be noted that the jet composition is currently uncertain. In addition to electrons and protons, there may be a certain number of other charged particles in the jet, such as positrons (e.g., Madejski et al. 2016). In a jet that satisfies the charge neutrality condition, the contribution from pp interactions would become weaker if there is a large number of positrons, thus making the model parameters more extreme. In this work, our main purpose is to study the maximum parameter space under the one-zone pp model, therefore we boldly assume that the charged particles in the jet are only relativistic and non-relativistic electrons and protons.

The following analytical calculation of searching the parameter space is under the framework of the conventional one-zone model. Assuming that all the observed jet’s non-thermal radiation comes from a single spherical region (hereafter, the blob) composed of a plasma of charged particles in a uniformly entangled magnetic field B with radius R and moving with the bulk Lorentz factor $\Gamma = \frac{1}{\sqrt{1-\beta^2}}$, where βc is the speed of the blob, at a viewing angle with respect to observers’ line of sight. For the relativistic jet close to the line of sight in blazars with a viewing angle of $\theta \lesssim 1/\Gamma$, we have the Doppler factor $\delta \approx \Gamma$. In this section, the parameters with superscript “obs” are measured in the observers’ frame, with superscript “AGN” are measured in the AGN frame, whereas the parameters without the superscript are measured in the comoving frame, unless specified otherwise.

2.1. Methods

For the hard-TeV spectrum, since the SSC emission cannot explain it because of the KN effect, we suppose that it can be interpreted by the γ -ray from π^0 decay produced in the pp interactions. The proton injection luminosity can be calculated as

$$L_{p,\text{inj}} = \frac{4}{3}\pi R^3 \langle \gamma_p \rangle m_p c^2 \dot{n}_p^{\text{inj}}, \quad (1)$$

where m_p is the rest mass of a proton, c is the speed of light,

$$\begin{aligned} \langle \gamma_p \rangle &= \frac{\int \gamma_p \dot{n}_p^{\text{inj}}(\gamma_p) d\gamma_p}{\dot{n}_p^{\text{inj}}} \\ &= \frac{(1 - \alpha_p)}{(2 - \alpha_p)} \left(\frac{\gamma_{p,\text{max}}^{2-\alpha_p} - \gamma_{p,\text{min}}^{2-\alpha_p}}{\gamma_{p,\text{max}}^{1-\alpha_p} - \gamma_{p,\text{min}}^{1-\alpha_p}} \right) \end{aligned} \quad (2)$$

represents the average proton Lorentz factor, where $\dot{n}_p^{\text{inj}}(\gamma_p) = \dot{n}_{0,p} \gamma_p^{-\alpha_p}$, $\gamma_{p,\text{min}} < \gamma_p < \gamma_{p,\text{max}}$ is the injection rate of proton energy distribution, $\dot{n}_{0,p}$ is the normalization in units of $\text{cm}^{-3} \text{ s}^{-1}$, α_p is the proton spectral index, γ_p is the proton Lorentz factor, $\gamma_{p,\text{min}}$ is the minimum proton Lorentz factor, and $\gamma_{p,\text{max}}$ is the maximum proton Lorentz factor, and $\dot{n}_p^{\text{inj}} = \int \dot{n}_p^{\text{inj}}(\gamma_p) d\gamma_p$ is the energy-integrated number density of injected relativistic protons. This pp explanation basically has two constraints, in which one is that the generated γ -ray luminosity from π^0 decay exceeds the

observed TeV luminosity², i.e.,

$$L_{\text{TeV}}^{\text{obs}} \leq L_{\text{p,inj}} f_{\pi_0} \delta^4, \quad (3)$$

where

$$f_{\pi_0} \approx \frac{1}{3} K_{\text{pp}} \sigma_{\text{pp}} n_{\text{H}} R \quad (4)$$

is the pp interaction efficiency, the factor $1/3$ is the branching ratio into π_0 , $\sigma_{\text{pp}} \approx 6 \times 10^{-26} \text{ cm}^2$ is the cross section for the pp interactions, n_{H} is the number density of cold protons in the jet and $K_{\text{pp}} \approx 0.5$ is the inelasticity coefficient (Kelner et al. 2006). The other constraint is that the total jet power that dominated by the power of relativistic and non-relativistic protons cannot exceed the Eddington luminosity of the SMBH, otherwise the growth of the SMBH would be too quick (Antognini et al. 2012). Therefore, we have

$$L_{\text{H}}^{\text{AGN}} + L_{\text{p,inj}}^{\text{AGN}} \leq L_{\text{Edd}}, \quad (5)$$

where $L_{\text{p,inj}}^{\text{AGN}} = L_{\text{p,inj}} \delta^2$ is the power of the injected relativistic protons in the AGN frame,

$$L_{\text{Edd}} = 2\pi m_{\text{p}} c^3 R_{\text{S}} / \sigma_{\text{T}} \quad (6)$$

is the Eddington luminosity of the SMBH, σ_{T} is the Thomson scattering cross section, $R_{\text{S}} = 2GM_{\text{BH}}/c^2$ is the Schwarzschild radius of the SMBH, M_{BH} is the SMBH mass and

$$L_{\text{H}}^{\text{AGN}} = \pi R^2 c \delta^2 m_{\text{p}} c^2 n_{\text{H}} \quad (7)$$

is the kinetic power in cold protons. In order to find the maximum parameter space, we assume that the π^0 decay generates the required minimum γ -ray luminosity, i.e., $L_{\text{TeV}}^{\text{obs}}$. Then, substituting $L_{\text{TeV}}^{\text{obs}} = L_{\text{p,inj}} f_{\pi_0} \delta^4$, Eq. 4, Eq. 6 and Eq. 7 into Eq. 5, we have

$$\frac{3\sigma_{\text{T}}}{\sigma_{\text{pp}}} \left(\frac{L_{\text{TeV}}^{\text{obs}}}{L_{\text{Edd}}} \right) \left(\frac{L_{\text{p,inj}}^{\text{AGN}}}{L_{\text{Edd}}} \right)^{-1} \left(\frac{R}{R_{\text{S}}} \right) + \frac{L_{\text{p,inj}}^{\text{AGN}}}{L_{\text{Edd}}} \leq 1. \quad (8)$$

If $L_{\text{p,inj}}^{\text{AGN}}$ is regarded as an independent variable, Eq. 8 becomes a quadratic formula. It can be found that the quadratic formula could get the minimum value when $L_{\text{p,inj}}^{\text{AGN}}$ is $L_{\text{Edd}}/2$. Then substituting $L_{\text{p,inj}}^{\text{AGN}} = L_{\text{Edd}}/2$ into Eq. 8, the maximum parameter space of R can be obtained through

$$\frac{R}{R_{\text{S}}} \leq \frac{\sigma_{\text{pp}}}{12\sigma_{\text{T}}} \frac{L_{\text{Edd}}}{L_{\text{TeV}}^{\text{obs}}}, \quad (9)$$

when the SMBH mass and TeV luminosity are measured.

In the above analytical calculations, by fixing the γ -ray luminosity from π^0 decay to the required minimum value, and keeping the total jet power not exceeding the Eddington luminosity of SMBH, the parameter space of R is well constrained. Similarly, the maximum parameter space of R can also be obtained by fixing the total jet power to the Eddington luminosity of SMBH, which is the maximum value that can be set, and making the γ -ray luminosity from π^0 decay larger than the observed TeV luminosity. Here, the power of the injected relativistic protons is considered as a fraction χ_{p} of the total jet power, which is

$$L_{\text{p,inj}}^{\text{AGN}} = \chi_{\text{p}} L_{\text{Edd}}. \quad (10)$$

² Since the intrinsic hard-TeV spectrum may not be truncated at the maximum energy currently observed, but will extend to higher energy, the theoretical luminosity should be larger than the current observed TeV luminosity.

Since the power of the relativistic and non-relativistic electrons is normally negligible compared to that of relativistic and non-relativistic protons, according to Eq. 7 and Eq. 10, n_{H} can be estimated as

$$n_{\text{H}} = \frac{(1 - \chi_{\text{p}}) L_{\text{Edd}}}{\pi R^2 \delta^2 m_{\text{p}} c^3}. \quad (11)$$

The γ -ray luminosity from π_0 decay produced in the pp interactions can be given by

$$L_{\gamma,\pi_0}^{\text{AGN}} \approx L_{\text{p,inj}}^{\text{AGN}} f_{\pi_0}. \quad (12)$$

Combining with Eq. 4, Eq. 10, Eq. 11 and Eq. 12, if the hard-TeV spectrum can be interpreted by the γ -ray from π_0 decay produced in the pp interactions, we can get

$$L_{\text{TeV}}^{\text{obs}} \leq L_{\gamma,\pi_0}^{\text{AGN}} = \frac{\sigma_{\text{pp}} \chi_{\text{p}} (1 - \chi_{\text{p}}) L_{\text{Edd}}^2}{6\pi m_{\text{p}} c^3 R}. \quad (13)$$

In order to get the maximum parameter space, it is necessary to set $\chi_{\text{p}} = 0.5$, which is consistent with the result obtained below Eq. 8. If further substituting Eq. 6 into Eq. 13, Eq. 9 can also be derived.

Xue et al. (2019a) collected a sample of hard-TeV BL Lacs with measured TeV luminosities and the SMBH masses. Their corresponding maximum R obtained by Eq. 9 are shown in Table 1. It can be seen that the derived maximum R is quite small which is comparable or even smaller than the Schwarzschild radius of the SMBH R_{S} . However, in such a compact blob, TeV photons are likely to be absorbed due to the internal $\gamma\gamma$ absorption. Since the spectra shape of soft photons is fixed by observational data points, i.e., the low energy component, the internal $\gamma\gamma$ absorption optical depth is only related to R and δ , i.e., $\tau_{\gamma\gamma} \propto R^{-1} \delta^{-4}$. Xue et al. (2019a) give the value of R and δ when $\tau_{\gamma\gamma}$ of the maximum energy of the hard-TeV spectrum is equal to unity. Therefore, in order to prevent the hard-TeV spectrum being absorbed, a larger δ must be introduced, since the maximum R shown in Table 1 is already much smaller than that given by Xue et al. (2019a). If the maximum δ that can be set is 30 as indicated by observation (Hovatta et al. 2009), only 1ES 0229+200 has a certain parameter space which can be used to interpret the hard-TeV spectrum with the one-zone pp model.

2.2. Charge neutrality condition of jet

Recently, Banik & Bhadra (2019) suggested that when considering the charge neutrality condition of blazar jet, there will be sufficient cold protons, making the pp interaction to be efficient and explaining the observed TeV γ -ray and neutrino emission from the blazar TXS 0506+056. However, if the kinetic power of cold protons is taken into account, a super-Eddington jet power is still needed since the blob radius introduced in their modeling is about a hundred times larger than that obtained by our analytical methods. In the following, we will investigate if the charge neutrality condition of jet can be satisfied when interpreting the hard-TeV spectra without introducing a super-Eddington jet power.

Due to the lack of the strong emission from external photon fields in TeV BL Lacs, it is generally accepted that the emission below $\sim 100 \text{ GeV}$ is originated from the synchrotron and SSC emission from primary relativistic electrons. The electron injection luminosity can be calculated as

$$L_{\text{e,inj}} = \frac{4}{3} \pi R^3 \langle \gamma_{\text{e}} \rangle m_{\text{e}} c^2 \dot{n}_{\text{e}}^{\text{inj}}, \quad (14)$$

Table 1. The sample of hard-TeV BL Lacs collected by [Xue et al. \(2019a\)](#).

Object	$L_{\text{TeV}}^{\text{obs}}$ (erg s ⁻¹)	$\text{Log}M_{\text{BH}}$ (M_{\odot})	R_s (cm)	R (cm)
1ES 0229+200	1.00×10^{45}	9.16 ± 0.11 (Meyer et al. 2012)	4.29×10^{14}	7.00×10^{14}
1ES 0347-121	1.63×10^{45}	8.02 ± 0.11 (Meyer et al. 2012)	3.10×10^{13}	2.25×10^{12}
1ES 0414+009	1.54×10^{45}	9	2.96×10^{14}	2.17×10^{14}
1ES 1101-232	1.02×10^{45}	9	2.96×10^{14}	3.30×10^{14}
1ES 1215+303	2.11×10^{45}	8.4 (Gupta et al. 2012)	7.45×10^{13}	1.00×10^{13}
1ES 1218+304	5.45×10^{45}	8.04 ± 0.24 (Meyer et al. 2012)	3.25×10^{13}	7.40×10^{11}
S5 0716+714	3.33×10^{46}	8 (Zdziarski & Bottcher 2015)	2.96×10^{13}	1.01×10^{11}
W Comae	6.00×10^{44}	8.7 (Zdziarski & Bottcher 2015)	1.49×10^{14}	1.41×10^{14}
TXS 0506+056	1.74×10^{45}	9	2.96×10^{14}	1.92×10^{14}

Notes. Columns from left to right: the source name; the observed luminosity of the TeV spectrum; logarithm of the SMBH mass in units of the solar mass, M_{\odot} ; the Schwarzschild radius of the SMBH; the maximum R obtained by Eq. 9.

where m_e is the rest mass of an electron,

$$\begin{aligned} \langle \gamma_e \rangle &= \frac{\int \gamma_e \dot{n}_e^{\text{inj}}(\gamma_e) d\gamma_e}{\dot{n}_e^{\text{inj}}} \\ &= \frac{(1 - \alpha_e)}{(2 - \alpha_e)} \left(\frac{\gamma_{e,\text{max}}^{2-\alpha_e} - \gamma_{e,\text{min}}^{2-\alpha_e}}{\gamma_{e,\text{max}}^{1-\alpha_e} - \gamma_{e,\text{min}}^{1-\alpha_e}} \right) \end{aligned} \quad (15)$$

is the average electron Lorentz factor, where $\dot{n}_e^{\text{inj}}(\gamma_e) = \dot{n}_{0,e} \gamma_e^{-\alpha_e}$, $\gamma_{e,\text{min}} < \gamma_e < \gamma_{e,\text{max}}$ is the injection rate of electron energy distribution (EED), $\dot{n}_{0,e}$ is the normalization in units of $\text{cm}^{-3} \text{s}^{-1}$, α_e is the electron spectral index, γ_e is the electron Lorentz factor, $\gamma_{e,\text{min}}$ is the minimum electron Lorentz factor, and $\gamma_{e,\text{max}}$ is the maximum electron Lorentz factor, and $\dot{n}_e^{\text{inj}} = \int \dot{n}_e^{\text{inj}}(\gamma_e) d\gamma_e$ is the energy-integrated number density of injected relativistic electrons. Taking into account cold electrons that are not accelerated or cooled, the total number density of electrons in the jet $n_{e,\text{tot}}$ can be approximated as

$$n_{e,\text{tot}} = \chi_e n_e, \quad (16)$$

where χ_e represents the ratio of $n_{e,\text{tot}}$ to n_e and

$$n_e \approx t_{\text{dyn}} \dot{n}_e^{\text{inj}} \quad (17)$$

is the number density of relativistic electrons, where $t_{\text{dyn}} = R/c$ is the dynamical timescale of the blob³.

Since the cooling of relativistic protons in the jet is inefficient, the number density of relativistic protons can be approximated as

$$n_p \approx t_{\text{dyn}} \dot{n}_p^{\text{inj}}. \quad (18)$$

Under the charge neutrality condition, combining Eq. 16 and Eq. 18, we get the number density of cold protons in the jet through

$$n_H = n_{e,\text{tot}} - n_p. \quad (19)$$

³ This relation comes from the fact that the radiative cooling of most electrons is in the slow cooling regime for BL Lacs. Although the cooling of high-energy electrons might be in the fast cooling regime, this result will not be significantly changed because the number density of relativistic electrons $n_{e,\text{rel}}$ is dominated by the low-energy electrons that dissipated in the slow cooling regime.

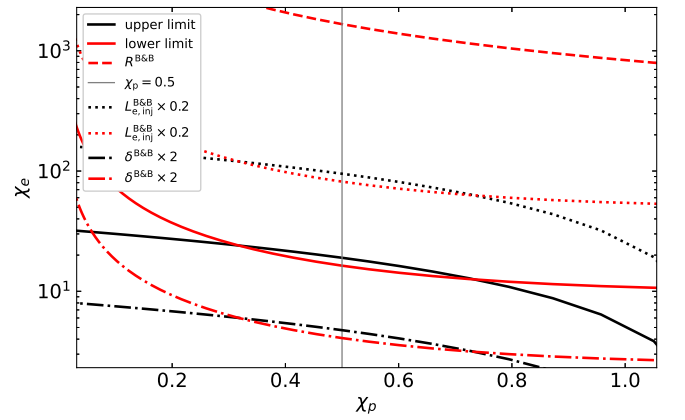


Fig. 1. The comparison of χ_e as a function of χ_p derived by Eq. 21 with different parameters. For all the line styles, the black and red curves represent the upper and lower limits, respectively. The solid curves are obtained when setting R as the maximum value given in Table 1 and values of other parameters as those provided by [Banik & Bhadra \(2019\)](#). Based on this, the dotted curves show the upper and lower limits when setting the electron injection luminosity as $L_{e,\text{inj}}^{\text{B\&B}} \times 0.2$, the dashed-dotted curves show the upper and lower limits when setting the Doppler factor as $\delta^{\text{B\&B}} \times 2$, and the dashed curve shows the lower limit when setting the blob radius as used in [Banik & Bhadra \(2019\)](#). The vertical line represents $\chi_p = 0.5$.

Substituting Eq. 1 and Eq. 14 into Eq. 19, we have

$$n_H = t_{\text{dyn}} \left(\frac{3\chi_e L_{e,\text{inj}}}{4\pi R^3 \langle \gamma_e \rangle m_e c^2} - \frac{3L_{p,\text{inj}}}{4\pi R^3 \langle \gamma_p \rangle m_p c^2} \right). \quad (20)$$

Further substituting Eq. 20 into Eq. 3 and Eq. 5, we can get

$$\frac{\langle \gamma_e \rangle m_e}{L_{e,\text{inj}} m_p} \left(4 \frac{\sigma_T}{\sigma_{\text{pp}}} \frac{R}{R_s} \frac{L_{\text{TeV}}^{\text{obs}}}{\chi_p \delta^2} + \frac{L_{p,\text{inj}}}{\langle \gamma_p \rangle} \right) \leq \chi_e \leq \langle \gamma_e \rangle \frac{L_{p,\text{inj}} m_e}{L_{e,\text{inj}} m_p} \left[\frac{4(1 - \chi_p)}{3\chi_p} + \frac{1}{\langle \gamma_p \rangle} \right]. \quad (21)$$

With the above inequalities, the range of χ_e satisfying the charge neutrality condition can be obtained. It is difficult to give a concise expression of the above inequalities, since the number density of relativistic electrons is greatly affected by the shape and energy range of EED, and $\gamma_{e,\text{min}}$ and $\gamma_{e,\text{max}}$ are poorly constrained in one-zone models. In any case, the above inequalities suggest that even though R is small, χ_e still has a parameter space

to satisfy the charge neutrality condition. Here we take TXS 0506+056 as an example. If we set R as its maximum value given in Table 1, and values of other parameters as those provided by Banik & Bhadra (2019)⁴, the range of χ_e as a function of χ_p that obtained by Eq. 21 is shown by the intersection area of black (upper limit) and red (lower limit) solid curves in Fig. 1. The vertical line in Fig. 1 marks the position of $\chi_p = 0.5$. It can be found that when $\chi_p = 0.5$, χ_e has largest range of value, which is consistent with the result obtained in Section 2.1. In addition, the comparison results of adjusting some other parameters are also shown in Fig. 1. It can be seen that adjusting the electron injection luminosity (dotted curves) and the Doppler factor (dashed-dotted curves) will change the parameter space of χ_e but the size of intersection area of the upper and lower limits remains the same. Also, when setting a larger blob radius $R^{\text{B\&B}} = 2.2 \times 10^{16}$ cm as used in Banik & Bhadra (2019), the lower limit represented by red dashed curve is much higher than the upper limit represented by black solid curve (since adjusting blob radius do not affect the upper limit, the black dashed curve is overlapped by the black solid curve), which suggest that a highly super-Eddington jet power has to be introduced.

3. Discussion and conclusion

In this work, we have investigated if one-zone pp models can explain the hard-TeV spectra of BL Lacs. With analytical calculations, we find that an extremely compact radiation region has to be assumed, if the hard-TeV spectrum is interpreted by γ rays produced from π_0 decay in pp interaction. However, if further considering the internal $\gamma\gamma$ opacity at TeV band is less than unity and the Doppler factor should be smaller than 30, only the hard-TeV spectra of 1ES 0229+200 can be explained. Even though, the allowable maximum radius of the blob under the constraints of Eq. 9 is very small, comparable to the Schwarzschild radius of the SMBH. This compact blob might be a relativistically moving plasmoid generated in the magnetic reconnection of the jet inside (Aharonian et al. 2017) and imply a fast minute-scale variability, which is observed in TeV band of radio galaxies (e.g., Aleksić et al. 2014) and blazars (e.g., Albert et al. 2007). However, no evidence of fast variability in TeV band of 1ES 0229+200 is found, therefore the injection of relativistic protons in such a compact blob must be continuous. On the other hand, it can be seen from Eq. 9 that for AGNs with low TeV luminosity, such as radio galaxies, the effective pp processes can occur in a large scale region (e.g., lobes) far from the SMBH, which could be a possible origin of the TeV spectrum (e.g., Sun et al. 2016).

In addition to conventional radiation models of blazars, another possible solution that invoked hypothetical conversion between axion-like particles (ALPs) and propagating γ -ray photons in an external magnetic field has been widely investigated on explaining the TeV emission of blazars (e.g., Sánchez-Conde et al. 2009). The conversion could enable propagating TeV-photons to avoid $\gamma\gamma$ absorption and thus lead to a very hard-TeV spectrum as observed (e.g., Long et al. 2020, 2021). If it takes place in the blob of the inner jet with a strong magnetic field, the effective conversion occurs on the order of GeV and the ALPs converted from the source photons cannot reconvert into photons in the lower Galactic magnetic-field (Tavecchio et al. 2015). As a result, a substantial part of GeV photons would be lost, and it may lead to the exceeded Eddington luminosity of the SMBH as well. Conversely, if it occurs in

the large-scale jet (also the TeV emission region) with a weaker magnetic field, this problem would be avoided.

In fact, the discovered different variability patterns between TeV emission and other wavelength emission of some hard-TeV BL Lacs may support the multi-zone origin of the hard-TeV spectra. For example, a TeV flare of the hard-TeV BL Lac 1ES 1215+303 was found by MAGIC in 2011, while no variability was found in the GeV band at the same time (Aleksić et al. 2012). Also, no fast variability in TeV band is found for many hard-TeV BL Lacs, while other wavelength emissions are highly variable (e.g., 1ES 0229+200; Aliu et al. 2014).

To summarize, we investigate the possibility that if the hard-TeV spectra of BL Lacs can be explained with the one-zone pp model, which complemented the completeness of the one-zone model in the study of the hard-TeV spectra of BL Lacs. Unfortunately, only 1ES 0229+200 can be explained at the cost of introducing a very small blob radius that is comparable to the Schwarzschild radius of SMBH. Therefore, combined with previous studies that applied other one-zone models, we suggest that any one-zone model cannot explain the hard-TeV spectra of BL Lacs generally. It should originate from multiple emitting regions (e.g., Yan et al. 2012). The region generating the emission below ~ 100 GeV and the region producing the hard-TeV spectrum should be decoupled (Wang et al. 2022b). Both leptonic and hadronic processes are possible to explain the hard-TeV spectrum of BL Lacs.

Acknowledgements. This work was supported by JSPS KAKENHI Grant JP19H00693. This work was supported in part by a RIKEN pioneering project "Evolution of Matter in the Universe (r-EMU)".

References

- Acciari, V. A., Aliu, E., Beilicke, M., et al. 2010, *ApJ*, 709, L163
 Ackermann, M., Ajello, M., Albert, A., et al. 2016, *Phys. Rev. Lett.*, 116, 151105
 Aharonian, F. A. 2000, *New A*, 5, 377
 Aharonian, F. A., Barkov, M. V., & Khangulyan, D. 2017, *ApJ*, 841, 61
 Albert, J., Aliu, E., Anderhub, H., et al. 2007, *ApJ*, 669, 862
 Aleksić, J., Alvarez, E. A., Antonelli, L. A., et al. 2012, *A&A*, 544, A142
 Aleksić, J., Ansoldi, S., Antonelli, L. A., et al. 2014, *Science*, 346, 1080
 Aliu, E., Archambault, S., Arlen, T., et al. 2014, *ApJ*, 782, 13
 Antognini, J., Bird, J., & Martini, P. 2012, *ApJ*, 756, 116
 Atoyan, A. M. & Dermer, C. D. 2003, *ApJ*, 586, 79
 Banik, P. & Bhadra, A. 2019, *Phys. Rev. D*, 99, 103006
 Bosch-Ramon, V., Perucho, M., & Barkov, M. V. 2012, *A&A*, 539, A69
 Böttcher, M., Reimer, A., Sweeney, K., et al. 2013, *ApJ*, 768, 54
 Blazewski, M., Sikora, M., Moderski, R., et al. 2000, *ApJ*, 545, 107
 Cerruti, M., Zech, A., Boisson, C., et al. 2015, *MNRAS*, 448, 910
 Chen, L. & Zhang, B. 2021, *ApJ*, 906, 105
 Das, S., Gupta, N., & Razaque, S. 2020, *ApJ*, 889, 149
 Deng, X.-J., Xue, R., Wang, Z.-R., et al. 2021, *MNRAS*, 506, 5764
 Dermer, C. D. & Schlickeiser, R. 1993, *ApJ*, 416, 458
 Essey, W., Ando, S., & Kusenko, A. 2011, *Astroparticle Physics*, 35, 135
 Ghisellini, G., Tavecchio, F., Maraschi, L., et al. 2014, *Nature*, 515, 376
 Gupta, S. P., Pandey, U. S., Singh, K., et al. 2012, *New A*, 17, 8
 Hillas, A. M. 1984, *ARA&A*, 22, 425
 Hovatta, T., Valtaoja, E., Tornikoski, M., et al. 2009, *A&A*, 494, 527
 IceCube Collaboration, Aartsen, M. G., Ackermann, M., et al. 2018, *Science*, 361, eaat1378
 Katarzyński, K., Ghisellini, G., Tavecchio, F., et al. 2006, *MNRAS*, 368, L52
 Kelner, S. R., Aharonian, F. A., & Bugayov, V. V. 2006, *Phys. Rev. D*, 74, 034018
 Liu, R.-Y., Wang, K., Xue, R., et al. 2019, *Phys. Rev. D*, 99, 063008
 Long, G. B., Lin, W. P., Tam, P. H. T., et al. 2020, *Phys. Rev. D*, 101, 063004
 Long, G., Chen, S., Xu, S., et al. 2021, *Phys. Rev. D*, 104, 083014
 Madejski, G. M., Nalewajko, K., Madsen, K. K., et al. 2016, *ApJ*, 831, 142
 Marscher, A. P. & Gear, W. K. 1985, *ApJ*, 298, 114
 Meyer, M., Raue, M., Mazin, D., et al. 2012, *A&A*, 542, A59
 Meyer, M., Montanino, D., & Conrad, J. 2014, *J. Cosmology Astropart. Phys.*, 2014, 003
 O'Sullivan, S. P. & Gabuzda, D. C. 2009, *MNRAS*, 400, 26
 Petropoulou, M. & Dermer, C. D. 2016, *ApJ*, 825, L11
 Prosekin, A., Essey, W., Kusenko, A., et al. 2012, *ApJ*, 757, 183

⁴ i.e., $\delta = 10$, $L_{e,\text{inj}} = 2.3 \times 10^{42}$ erg/s, $\gamma_{e,\text{min}} = 1$, $\gamma_{e,\text{max}} = 1.5 \times 10^5$, $\alpha_e = 1.71$, $\gamma_{p,\text{min}} = 1$, $\gamma_{p,\text{max}} = 1.1 \times 10^7$, $\alpha_p = 2.13$.

- Sahu, S., López Fortín, C. E., & Nagataki, S. 2019, *ApJ*, 884, L17
- Sahakyan, N. 2018, *ApJ*, 866, 109
- Sánchez-Conde, M. A., Paneque, D., Bloom, E., et al. 2009, *Phys. Rev. D*, 79, 123511
- Sikora, M., Begelman, M. C., & Rees, M. J. 1994, *ApJ*, 421, 153
- Sun, X.-. na ., Yang, R.-. zhi ., Mckinley, B., et al. 2016, *A&A*, 595, A29
- Tavecchio, F., Roncadelli, M., & Galanti, G. 2015, *Physics Letters B*, 744, 375
- Takami, H., Murase, K., & Dermer, C. D. 2016, *ApJ*, 817, 59
- Tan, C., Xue, R., Du, L.-M., et al. 2020, *ApJS*, 248, 27
- Urry, C. M. & Padovani, P. 1995, *PASP*, 107, 803
- Wang, Z.-R. & Xue, R. 2022, *Research in Astronomy and Astrophysics*, 21, 305
- Wang, Z.-R., Liu, R.-Y., Petropoulou, M., et al. 2022, *Phys. Rev. D*, 105, 023005
- Xue, R., Liu, R.-Y., Wang, X.-Y., et al. 2019, *ApJ*, 871, 81
- Xue, R., Liu, R.-Y., Petropoulou, M., et al. 2019, *ApJ*, 886, 23
- Xue, R., Liu, R.-Y., Wang, Z.-R., et al. 2021, *ApJ*, 906, 51
- Yan, D., Zeng, H., & Zhang, L. 2012, *MNRAS*, 424, 2173
- Zdziarski, A. A. & Bottcher, M. 2015, *MNRAS*, 450, L21